Vibrational predissociation dynamics of methane–Ar: an *ab initio* approach

Michel Geleijns,[a] Nadine Halberstadt,[b] Judith Millan,†[b] Paul E. S. Wormer[a] and Ad van der Avoird[a]

[a] *Institute of Theoretical Chemistry, NSR-Center, University of Nijmegen, Toernooiveld, 6525 ED Nijmegen, The Netherlands. E-mail: avda@theochem.kun.nl*
[b] *Laboratoire de Physique Quantique, IRSAMC, CNRS and Université Paul Sabatier, 31062 Toulouse, France*

Received 5th December 2000
First published as an Advance Article on the web 5th June 2001

We calculated the cross sections for vibrational predissociation of methane–Ar induced by excitation of the methane ν_3 mode with the aid of an *ab initio* CH_4–Ar potential depending explicitly on the ν_3 and ν_1 normal coordinates of the CH_4 monomer. We found that dissociation into CH_4 fragments excited in the ν_1 mode, a $V \rightarrow V'$ process with very low kinetic energy release, strongly dominates over direct dissociation into Ar and ground state CH_4, and is responsible for the line broadening observed experimentally. The (observed and calculated) strong variation of the line widths for the Van der Waals levels excited in combination with the ν_3 mode (giving states of A, F and E symmetry) is related to the opening up of appropriate ν_1 dissociation channels and the occurrence of rotational resonances in the ν_1 continuum in the energy range of the quasi-bound ν_3 levels.

1 Introduction

Important dynamical phenomena that occur during molecular collisions in gases or liquids, such as vibrational and rotational energy transfer and relaxation, can be investigated in great detail by studying the photodissociation of a Van der Waals complex. This 'half-collision' is initiated by photo-excitation of one of the constituent molecules in the complex to a well-defined vibrational state, possibly in combination with the excitation of specific intermolecular (librational or translational) modes of the complex. Then the redistribution of the excitation energy over the intra- and intermolecular degrees of freedom can be monitored. The various possible decay processes can be followed either by time-resolved spectroscopic studies, or by determination of lifetimes from the line widths in the excitation spectrum. The recoil angles, velocities, and state distributions of the fragments can be obtained by further spectroscopic probing. This type of study is especially interesting for complexes containing polyatomic molecules. The vibrational predissociation of such a complex can occur not only by a simple $V \rightarrow R$, T (vibration to rotation and translation) transfer but also by partial transfer of the initial vibrational energy to other vibrational modes of the polyatomic ($V \rightarrow V'$, R, T transfer).

† Permanent address: Centro Científico Tecnológico, Departamento de Química, Universidad de la Rioja, Madre de Dios 51, 26006 Logroño, Spain.

DOI: 10.1039/b009741l

An essential element of theoretical studies aimed at understanding the observed phenomena is an intermolecular potential surface with an explicitly given dependence on the intramolecular (vibrational) coordinates of the constituents. Mostly,[1–3] such a surface is modeled by using a simple atom–atom potential. Apart from the question of its (in)accuracy, in general, it is important in this context that the assumption that the atom–atom model more or less correctly describes the intramolecular coordinate dependence of an intermolecular potential has never been suitably tested. Bissonnette and Clary[4] avoid this assumption in their theoretical study of H_2O–Ar which accompanies the experimental work of Nesbitt and Lascola.[5,6] They modeled the dependence of the H_2O–Ar potential on the internal coordinates of H_2O by considering only the dipole and quadrupole induction terms. Since it is possible nowadays to obtain quite accurate intermolecular potentials from *ab initio* electronic structure computations,[7] it is worthwhile to verify whether such calculations can also yield accurate results for the coupling in the potential between the inter- and intramolecular degrees of freedom.

Both of the above problems, regarding the predissociation dynamics and the dependence of the intermolecular potential on the molecular vibration coordinates, are addressed in this paper. The prototype system that we have chosen to investigate is CH_4–Ar. The measured infrared spectrum of methane–Ar was first presented and discussed at the previous Faraday Discussion on Van der Waals molecules, without an assignment or interpretation, however.[8–10] Later it was demonstrated[11,12] that this spectrum can be understood and assigned by means of *ab initio* calculations. The calculation of the spectrum was based on a potential obtained from *ab initio* symmetry-adapted perturbation theory (SAPT).[13] The same potential produced accurate elastic (total differential) and rotationally inelastic (state-to-state integral) cross sections for methane–Ar scattering.[13,14] The different bands observed in the infrared spectrum correspond to excitation of the ν_3 mode of methane, in combination with several intermolecular vibrations. The spectrum is quite complex since the occurrence of different nuclear spin species, A, F and E, causes several initial states to be populated even at the low temperature ($\approx$1 K) of the experiment. The degree of hindrance of the CH_4 rotations in the complex varies considerably: nearly free internal rotor states occur for the A and F species, whereas relatively large splittings of the free rotor levels are found for the E species with nonzero values of the rotational quantum number K. The CH_4–Ar complex is a very interesting system with regard to the problems mentioned in the first paragraph. It was observed in the IR spectrum reported by Miller *et al.*[11,12] that the bands which correspond to the excitation of different nuclear spin species and different intermolecular levels, although different in energy by only a few cm^{-1}, show vibrational predissociation line widths that vary by an order of magnitude.

The present paper describes a theoretical study of the photodissociation of methane–Ar, with the aim of understanding the large variation of the observed lifetimes and predicting the corresponding fragment state distributions (yet to be measured). We consider the fragmentation of the complex into two different channels, after excitation of the methane ν_3 mode. The first channel leads directly to Ar and ground state CH_4. In the second channel the CH_4 fragment remains excited in the ν_1 mode. Since the ν_3 vibration is only 103 cm^{-1} higher in energy than the ν_1 mode and the dissociation energy D_0 of the complex[11] is about 90 cm^{-1} this channel is barely open. Therefore, the complex can dissociate into this channel with very small kinetic energy release which, according to the energy gap law,[15,16] is likely to be a fast process. In Section 2 we present the results of *ab initio* SAPT calculations of a CH_4–Ar potential with explicit dependence on the ν_3 (asymmetric C–H stretch) and ν_1 (symmetric C–H stretch) normal coordinates of CH_4. The dependence of the intermolecular potential on both these normal modes was fit to an analytic expression. For the threefold degenerate ν_3 mode we did not need to compute all the components, but we used the transformation properties of the permutation-inversion symmetry group $PI(T_d)$ of the complex to obtain the complete ν_3 coupling term in the potential. In Section 3 it is outlined how we determined resonances in the energy-dependent cross section for vibrational predissociation into both channels. Complications, again, are the threefold degeneracy of the ν_3 mode and the first order Coriolis coupling of the vibrational angular momentum generated by this mode with the (hindered) internal rotation of CH_4 in the complex. Inclusion of this rather small coupling term is necessary to obtain the correct symmetry selection rules for the transitions. The direct calculation of the spectral line widths by a Fermi golden rule formula is also described in Section 3. In Section 4 we discuss the results.

2 Potential energy surface

We computed the potential as a function of the argon spherical polar coordinates R, Θ, Φ and the CH_4 vibrational stretching modes by the same SAPT (symmetry adapted perturbation theory) method as in previous work.[13] The same atomic orbital basis set was also used. In ref. 13 methane was considered in its vibrational ground state only, whereas in this work we will present the dependence of the argon–methane potential on the CH_4 stretch coordinates as well. The vibrational symmetry coordinates are linear combinations of the stretches[17]

$$\delta r_i \equiv \boldsymbol{a}_i/a \cdot (\boldsymbol{d}_i - \boldsymbol{d}_C), \tag{1}$$

where $\boldsymbol{d}_i$ and $\boldsymbol{d}_C$ are displacement coordinates of hydrogen i and the carbon atom, respectively. The vector $\boldsymbol{a}_i$ is along the equilibrium C–H bond and its length a is the equilibrium bond length. The point group of methane is T_d which has irreps (irreducible representations): $A_{1,2}$, E and $F_{1,2}$. The PI group $PI(T_d)$ of CH_4 and CH_4–Ar, which consists of permutation-inversions (PIs), is isomorphic to this point group. The symmetric (A_1) ν_1 stretch coordinate is designated by q_1 and the coordinates of the three-fold degenerate ν_3 mode spanning the irrep F_2 are q_{3x}, q_{3y}, q_{3z}. The symmetry adapted linear combinations are:

$$q_1 = (\delta r_1 + \delta r_2 + \delta r_3 + \delta r_4)/2, \tag{2}$$

and

$$\begin{aligned} q_{3x} &= (-\delta r_1 + \delta r_2 + \delta r_3 - \delta r_4)/2, \\ q_{3y} &= (-\delta r_1 + \delta r_2 - \delta r_3 + \delta r_4)/2, \\ q_{3z} &= (\delta r_1 + \delta r_2 - \delta r_3 - \delta r_4)/2. \end{aligned} \tag{3}$$

These modes correspond to methane in a cube with proton 1 on the $(-1, -1, 1)$ corner, proton 2 on the $(1, 1, 1)$ corner, proton 3 on the $(1, -1, -1)$ corner, and proton 4 on the $(-1, 1, -1)$ corner. The three bending ν_4 coordinates of methane span the same T_d irrep F_2 as the ν_3 stretch coordinates and the two sets of coordinates mix in Wilson's harmonic GF method.[18] However, in this work we make the simplifying assumption that the ν_3 coordinates are pure stretch modes and that both ν_1 and ν_3 are harmonic.

The displacement vector associated with the translational Eckart conditions has symmetry F_2,[19] which implies that we must not only change the C–H bond lengths in the ν_3 deformation, as we do in the ν_1 deformation, but we must also move the carbon position. Since the vector associated with the rotational Eckart conditions has symmetry F_1, both the ν_1 and ν_3 deformations automatically satisfy these conditions.

The action of PIs on the symmetry coordinates is simply

$$\hat{P}(q_{3x}, q_{3y}, q_{3z}) = (q_{3x}, q_{3y}, q_{3z})\mathscr{R}(P), \quad P \in PI(T_d), \tag{4}$$

where $\mathscr{R}(P)$ is a matrix in the orthogonal irrep F_2.

To consider the action of the PIs on the Euler angles we define a body-fixed frame for the equilibrium methane, which is the equivalent of eqn. (3),

$$\begin{aligned} g_x &= (-\overrightarrow{OH}_1 + \overrightarrow{OH}_2 + \overrightarrow{OH}_3 - \overrightarrow{OH}_4)/2 \\ g_y &= (-\overrightarrow{OH}_1 + \overrightarrow{OH}_2 - \overrightarrow{OH}_3 + \overrightarrow{OH}_4)/2 \\ g_z &= (\overrightarrow{OH}_1 + \overrightarrow{OH}_2 - \overrightarrow{OH}_3 - \overrightarrow{OH}_4)/2 \end{aligned} \tag{5}$$

This frame is in terms of vectors pointing from the center of mass O of methane to hydrogen atoms H_i. The Euler angles ω of methane are defined by

$$(g_x, g_y, g_z) = (f_x, f_y, f_z)\mathscr{R}(\omega) = (f_x, f_y, f_z)\mathscr{R}_z(\omega_1)\mathscr{R}_y(\omega_2)\mathscr{R}_z(\omega_3) \tag{6}$$

where (f_x, f_y, f_z) is a two-angle embedded frame obtained by rotating an arbitrary space-fixed frame so that f_z lies along $\boldsymbol{R}$, the vector pointing from the center of mass of CH_4 to Ar. The Euler rotation matrices are in the active convention, see, *e.g.* ref. 20. It is not difficult to show that the Eckart frame (according to the definition of ref. 20) of methane deformed along q_{3z} is the same as the frame in eqn. (5). So we can use this frame to study the effect of the PIs on the Euler angles. The PIs act on these angles according to

$$\hat{P}(g_x, g_y, g_z) = (g_x, g_y, g_z)\mathscr{S}(P) = (f_x, f_y, f_z)\mathscr{R}(\omega)\mathscr{S}(P) = (f_x, f_y, f_z)\mathscr{R}(\omega'). \tag{7}$$

The permutations act on the hydrogen labels and E^* inverts the direction of the g_α so that the computation of the matrices $\mathscr{S}(P)$ is straightforward. In fact they form the F_1 irrep, which consists of proper (unit determinant) rotation matrices only and accordingly ω' is well-defined. Note that E^* is equivalent[11] to a rotation of the two-angle embedded frame by $\mathscr{R}_z(\pi)\mathscr{R}_y(\pi)$.

In order to obtain the dependence of the potential on the four C–H stretch coordinates it is sufficient to consider deformations of methane along q_1 and q_{3z} only. The dependence on the other two coordinates can be obtained by appropriate permutation of the hydrogen atoms. Since the q_{3z} deformation lowers the point group symmetry of CH_4 to C_{2v}, six times more points on the potential energy surface (PES) must be computed than in the case of undeformed methane. At the same time we must describe the PES in functions containing A_1 symmetry of C_{2v}—and not A_1 of T_d, as in earlier work.[11,13] We fitted the *ab initio* SAPT points in a somewhat different manner than before. All short range terms, including penetration induction, are taken together and the sum is written as

$$V_{\text{short}}(R, \Theta, \Phi, q_1, \boldsymbol{q}_3) = \left[\sum_{l,\gamma}^{l_{\max}=7} \sum_{n=0}^{3} A^{\text{short}}_{l,\gamma,n} T^{(l)}_\gamma(\Theta, \Phi) R^n\right] \exp\left[-\sum_{l,\gamma}^{l_{\max}=7} \alpha^{\text{short}}_{l,\gamma} T^{(l)}_\gamma(\Theta, \Phi) R\right], \tag{8}$$

where $\boldsymbol{q}_3 \equiv (q_{3x}, q_{3y}, q_{3z})$. The functions $T^{(l)}_\gamma(\Theta, \Phi)$ are tetrahedral harmonics belonging to irreps of T_d. The index γ is compound, it labels the T_d irrep, the partner in this irrep and the multiplicity. The $T^{(l)}_\gamma(\Theta, \Phi)$ are linear combinations of spherical harmonics of certain l

$$T^{(l)}_\gamma(\Theta, \Phi) = \sum_m Z^{lm}_\gamma Y^l_m(\Theta, \Phi), \tag{9}$$

where the algebraic coefficients Z^{lm}_γ may be found in ref. 21. Only the irreps A_1, E and F_2 of T_d appear here, since only those irreps contain A_1 of C_{2v}. The exponential parameters $\alpha^{\text{short}}_{l,\gamma}$ were obtained from a fit of the CH_4–Ar potential with methane in its vibrational ground state and were kept fixed. That is, the tetrahedral harmonics appearing in the exponent are A_1 under T_d. The coefficients $A^{\text{short}}_{l,\gamma,n}$ are obtained from least squares fits with methane deformed along q_{3z} and q_1. The long range interaction only consists of dispersion (the long range induction being negligibly small), which we represent by the analytic form

$$\begin{aligned} V_{\text{disp}}(R, \Theta, \Phi, q_1, \boldsymbol{q}_3) = &\left[\sum_{l,\gamma}^{l_{\max}=7} \sum_{n=0}^{3} A^{\text{disp}}_{l,\gamma,n} T^{(l)}_\gamma(\Theta, \Phi,) R^n\right] \exp[-\alpha^{\text{disp}} R] \\ &- \sum_{l,\gamma}^{l_{\max}=7} \sum_{n=6}^{10} f_n(R; \alpha^{\text{disp}}) C^{\text{disp}}_{l,y,n} T^{(l)}_\gamma(\Theta, \Phi) R^{-n} \end{aligned} \tag{10}$$

The Van der Waals coefficients $C^{\text{disp}}_{l,\gamma,n}$ were computed separately for deformed methane by the program POLCOR,[22] at the same correlation level as the SAPT dispersion. The exponential fit parameter α^{disp} is determined for the undeformed methane and kept constant. It appears also in damp functions that have the Tang–Toennies form,[23]

$$f_n(R; b) = 1 - \exp(-bR) \sum_{k=0}^{n} \frac{(bR)^k}{k!} \tag{11}$$

The parameters $A^{\text{disp}}_{l,\gamma,n}$ are obtained by a fit of the SAPT dispersion energy computed for nine deformations of methane, in the same way as the $A^{\text{short}}_{l,\gamma,n}$ are obtained from a fit of the short range

energies. The linear parameters A^{short}, A^{disp} and C^{disp} in the fits were taken to be functions of the normal coordinates. Writing generically A for these linear parameters, we make a Taylor expansion around equilibrium and include only the coupling terms which we will need later, namely

$$A(q_1, \boldsymbol{q}_3) = A(0) + \left(\frac{\partial A}{\partial q_1}\right)_0 q_1 + \sum_\alpha \left(\frac{\partial A}{\partial q_{3\alpha}}\right)_0 q_{3\alpha} + \sum_\alpha \left(\frac{\partial^2 A}{\partial q_{3\alpha}\partial q_1}\right)_0 q_{3\alpha} q_1. \tag{12}$$

The derivatives in this expansion are parameters obtained from the potential on the following grid of deformations: $(\Delta q_1, \Delta q_{3z}) = (0, 0), (1, -1), (1, 0), (1, 1), (0, 1), (-1, 1), (-1, 0), (-1, -1)$ and $(0, -1)$, where Δq_1 has the unit of length 0.199 a_0; for Δq_{3z} this length is 0.205 a_0. These lengths are obtained from the classical turning points in the force field of ref. 24. We experimented with different lengths of the Taylor expansion, but variation in the expansion lengths hardly affected the numerical values of the coupling terms of interest.

Note incidentally that a number of *ab initio* SAPT calculations can be skipped because of the relation obtained by the application of (1324)*:

$$E^{\text{SAPT}}(\Delta q_{3z}, R, \Theta, \Phi) = E^{\text{SAPT}}(-\Delta q_{3z}, R, \pi - \Theta, \pi/2 + \Phi).$$

The effect of the deformations Δq_{3z} and $\Delta q_{3z} + \Delta q_1$ on the potential is illustrated in Fig. 1 and 2.

The fit of E^{SAPT} values calculated for methane deformed along q_{3z} and q_1 fixes the three parameters: $(\partial A/\partial q_1)_0$, $(\partial A/\partial q_{3z})_0$ and $(\partial^2 A/\partial q_{3z}\partial q_1)_0$. In order to show how to obtain the correspond-

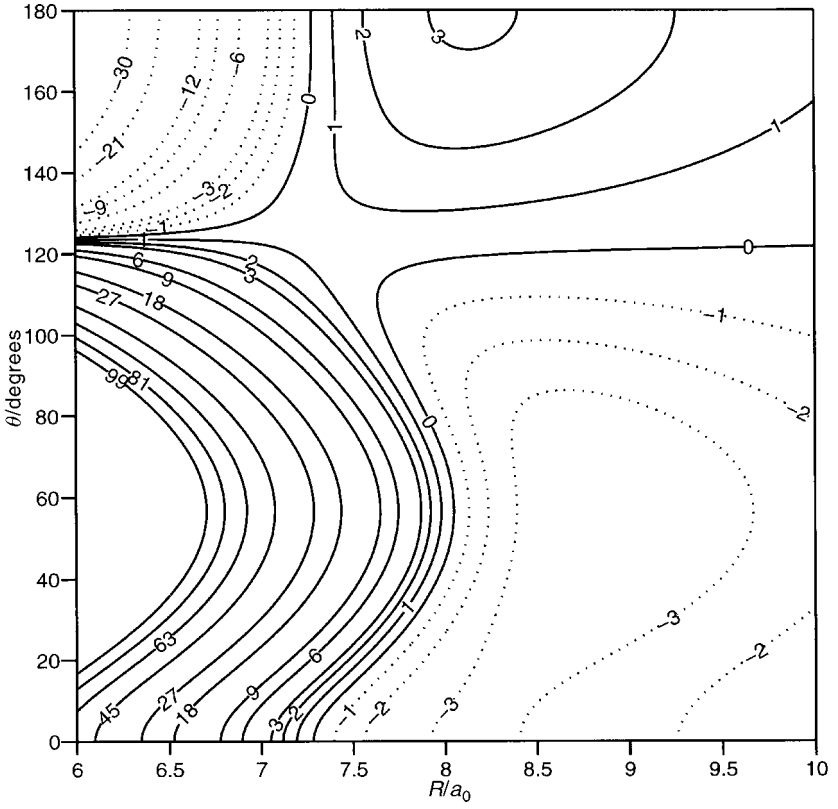

Fig. 1 Effect of ν_3 mode deformation on the CH_4–Ar potential (in cm^{-1}): $E^{\text{SAPT}}(\Delta q_{3z}) - E^{\text{SAPT}}(0)$ with $\Delta q_{3z} = 0.205\ a_0$. The azimuthal angle $\Phi = 45°$. Note that $\Theta = 54.74°$ corresponds to a vertex position of argon (a linear C–H···Ar configuration), $\Theta = 125.26°$ to a facial position (between three C–H bonds), and $\Theta = 0°$ and 180° to edge positions (Ar, C and two H atoms in one plane).

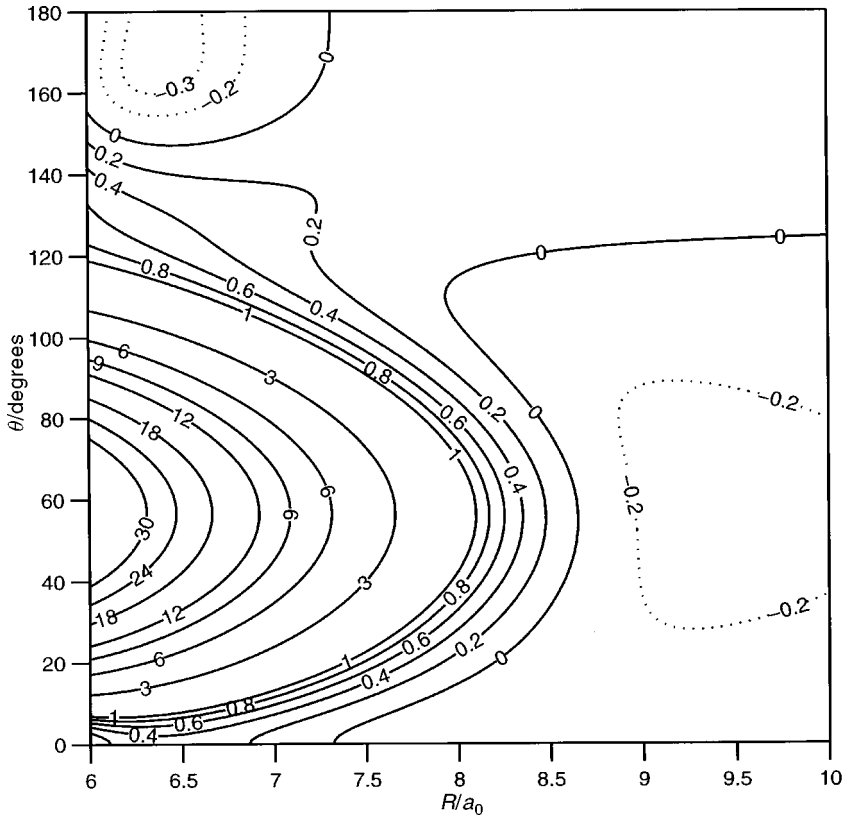

Fig. 2 Effect of simultaneous ν_3 and ν_1 mode deformation on the CH_4–Ar potential (in cm^{-1}): $E^{SAPT}(\Delta q_{3z}, \Delta q_1) - E^{SAPT}(\Delta q_{3z}) - E^{SAPT}(\Delta q_1) + E^{SAPT}(0)$ with $\Delta q_{3z} = 0.205\ a_0$ and $\Delta q_1 = 0.199\ a_0$. See the caption of Fig. 1 for explanations.

ing derivatives in the other directions, we reintroduce the labels l and γ on the A's and define the function

$$B^l_m(q_1, \boldsymbol{q}_3) = \sum_\gamma A_{l,\gamma}(q_1, \boldsymbol{q}_3) Z^{lm}_\gamma, \tag{13}$$

where $A_{l,\gamma}$ is any of the three linear parameters under discussion and where we suppressed the label n and the type designation ('short' *etc.*). In the potential expansion we now meet the functions

$$V^l(q_1, \boldsymbol{q}_3, \Theta, \Phi) \equiv \sum_m B^l_m(q_1, \boldsymbol{q}_3) Y^l_m(\Theta, \Phi) \tag{14}$$

which are invariant under $PI(T_d)$, provided we act *simultaneously* on q_1, $\boldsymbol{q}_3$, Θ and Φ.

Let us first consider the normal modes and substitute into eqn. (4) $\hat{P} = (134)$. Upon noticing that $\hat{P}q_1 = q_1$ and $\hat{P}\boldsymbol{q}_3 = (q_{3y}, q_{3z}, q_{3x})$ we find

$$\begin{aligned}\hat{P}B^l_m(q_1, \boldsymbol{q}_3) = B^l_m(0) &+ \left(\frac{\partial B^l_m}{\partial q_1}\right)_0 q_1 + \left(\frac{\partial B^l_m}{\partial q_{3x}}\right)_0 q_{3y} + \left(\frac{\partial B^l_m}{\partial q_{3y}}\right)_0 q_{3z} + \left(\frac{\partial B^l_m}{\partial q_{3z}}\right)_0 q_{3x} \\ &+ \left(\frac{\partial^2 B^l_m}{\partial q_{3x}\,\partial q_1}\right)_0 q_{3y} q_1 + \left(\frac{\partial^2 B^l_m}{\partial q_{3y}\,\partial q_1}\right)_0 q_{3z} q_1 + \left(\frac{\partial^2 B^l_m}{\partial q_{3z}\,\partial q_1}\right)_0 q_{3x} q_1. \end{aligned} \tag{15}$$

We now look at the action of $\hat{P} = (134)$ on the Euler angles. Since this is an unstarred operation it acts in exactly the same way on the body-fixed axes g_α as on the $q_{3\alpha}$. Implicitly we already used

the left-hand side of the following equation and the right-hand side follows by inspection:

$$\mathscr{S}(134) = \begin{pmatrix} 0 & 0 & 1 \\ 1 & 0 & 0 \\ 0 & 1 & 0 \end{pmatrix} = \mathscr{R}_y(\pi/2)\mathscr{R}_z(\pi/2). \tag{16}$$

From eqn. (7) we find the relation between ω' and ω. Earlier[11] it was shown that, instead of rotating CH_4 inside the complex, we may rotate the position vector of the argon atom, while keeping the orientation of methane fixed. The rotation angles ω of the monomer are simply related to the angles Θ and Φ by $\omega_2 \equiv \Theta$ and $\omega_3 \equiv \pi - \Phi$. It is now easy to find the effect of $\hat{P}$ on the spherical polar angles of $\boldsymbol{R}$, and for the functions we get the transformation:

$$Y^l_{m'}(\Theta', \Phi') = \sum_m Y^l_m(\Theta, \Phi) D^{(l)}_{mm'}(\mathscr{S}(134)) = \sum_m Y^l_m(\Theta, \Phi) D^{(l)}_{mm'}(0, \pi/2, \pi/2). \tag{17}$$

Substitution of this expression and eqn. (15) into V^l, use of $\hat{P}V^l = V^l$, and equating of terms in $q_{3\alpha}$ and $Y^l_m(\Theta, \Phi)$ gives the expressions

$$\left(\frac{\partial B^l_m}{\partial q_{3x}}\right)_0 = \sum_{m'} \left(\frac{\partial B^l_{m'}}{\partial q_{3z}}\right)_0 D^{(l)}_{mm'}(0, \pi/2, \pi/2),$$

$$\left(\frac{\partial B^l_m}{\partial q_{3y}}\right)_0 = \sum_{m'} \left(\frac{\partial B^l_{m'}}{\partial q_{3x}}\right)_0 D^{(l)}_{mm'}(0, \pi/2, \pi/2), \tag{18}$$

Knowing $(\partial B^l_m/\partial q_{3z})_0$ from the fits, these expressions are easily solved sequentially. Likewise

$$\left(\frac{\partial^2 B^l_m}{\partial q_{3x}\,\partial q_1}\right)_0 = \sum_{m'} \left(\frac{\partial^2 B^l_{m'}}{\partial q_{3z}\,\partial q_1}\right)_0 D^{(l)}_{mm'}(0, \pi/2, \pi/2), \tag{19}$$

and two other expressions with x, y, z permuted cyclically.

3 Photodissociation formalism

The cross section for excitation of a system from an initial bound state $|\Psi_i\rangle$ with discrete energy E_i to the continuum state $|\Psi_f(E)\rangle$ is given by

$$\sigma_{f\leftarrow i}(E) \propto |\langle \Psi_f(E)|\, \boldsymbol{\mu}\cdot\boldsymbol{e}\,|\Psi_i\rangle|^2. \tag{20}$$

Here $\boldsymbol{e}$ is the polarization vector of the incoming photon and $\boldsymbol{\mu}$ is the dipole moment surface. With the photon having energy $\hbar\omega$, energy conservation gives $E = E_i + \hbar\omega$. In the present work we generalize the atom–diatom formalism of Roncero *et al.*[25] to atom–polyatom systems with different monomer modes, part of which are degenerate. The bound state $|\Psi_i\rangle$ is one of the Van der Waals states of the dimer in its vibrational ground state. Because of nuclear spin there are three types of intermolecular vibrational ground states: A, E and F. All three are occupied in supersonic molecular beams. Since these beams are cold (about 1 K), hardly any excited Van der Waals states are occupied. The final state is a ν_3 state which is coupled with the continuum states of the ground state potential as well as of the ν_1 potential. In the present work we assume that the ν_3 and ν_1 potentials are the same as the ground state potential, but shifted upward by 3019.494 and 2916.480 cm^{-1}, respectively, which are the band origins of the ν_3 and ν_1 levels in free CH_4.[26]

The nuclear Hamiltonian in the dimer embedded frame is

$$H = H_A(q_1, \boldsymbol{q}_3) + T_A + \frac{1}{2\mu R^2}\left[-\hbar^2 \frac{\partial}{\partial R} R^2 \frac{\partial}{\partial R} + (J^{tot})^2 + j^2 - 2\boldsymbol{j}\cdot\boldsymbol{J}\right] + V(R, \omega_2, \omega_3, q_1, \boldsymbol{q}_3), \tag{21}$$

where T_A is the kinetic energy of CH_4, $(J^{tot})^2$ is the total angular momentum of the complex, $\boldsymbol{J} = \mathscr{R}(\alpha, \beta)^T \boldsymbol{J}^{tot}$, and $\boldsymbol{j}$ is the (space-fixed) angular momentum operator of methane. The operator j^2 is this operator squared. The angles α and β are the usual spherical polar angles of $\boldsymbol{R}$ with respect to an arbitrary space-fixed frame. The term $H_A(q_1, \boldsymbol{q}_3)$, the harmonic oscillator Hamiltonian of methane, is taken into account effectively by the shifts of the potentials of the ν_3 and ν_1 excited states. Finally μ is the reduced mass of the dimer. Note that $(J^{tot})^2$ and its projection J_z on

the space-fixed z-axis are constants of the motion with conserved quantum numbers J and M, respectively. The only terms that break K, which is the projection of $\boldsymbol{J}$ and $\boldsymbol{j}$ on $\boldsymbol{R}$, are the cross terms in $\boldsymbol{j}\cdot\boldsymbol{J}$. For low J this part of the Coriolis interaction is very small and we omit it from our calculations. Hence we take K to be conserved. (Note that the K quantum number is often designated by Ω in scattering papers).

In the ground and ν_1 vibrational states of CH_4 we simply have the spherical top Hamiltonian for the free methane, namely $T_A = B_v\, j^2$. In the vibrationally excited ν_3 mode there is first-order Coriolis coupling between the vibrational angular momentum $\boldsymbol{l}^{vib}$ and the body-fixed angular momentum $\boldsymbol{j}^{BF}$ of methane.[19] That is, when the molecule is in the ν_3 mode, the kinetic energy T_A takes the form

$$T_A = B_3\, j^2 - 2\zeta_3\, B_3\, \boldsymbol{l}^{vib}\cdot\boldsymbol{j}^{BF}. \tag{22}$$

The ν_3 functions, $|\nu_3, m_l\rangle$, are eigenfunctions of the operator $(l^{vib})^2$ with eigenvalue $l(l+1)$ with $l = 1$ and of l_z^{vib} with eigenvalues $m_l = -1$, 0 and 1, respectively. These eigenfunctions behave in the usual manner under the step-up and step-down operators $l_\pm^{vib}$. Although the Coriolis parameter, ζ_3, can be obtained from a normal mode analysis, in this work we used an experimental value, as is also the case for the monomer rotational constants B_v. The rotational constants of the monomer were $B_0 = 5.241\,035\,6$ cm^{-1} for the ground state,[27] $B_1 = 5.197\,16$ cm^{-1} for the ν_1 state,[28] and $B_3 = 5.199\,70$ cm^{-1} for the ν_3 state.[24] The Coriolis parameter[24] ζ_3 was fixed at 0.055 33 and the following masses[29] were used, ^{40}Ar: 39.9627 u, ^{1}H: 1.007 825 u and ^{12}C: 12 u.

In our scattering and bound state calculations we used the following angular and vibrational body-fixed basis:

$$|v, j, k, K\rangle = \sqrt{\frac{(2j+1)(2J+1)}{32\pi^3}}\, D^{(j)}_{Kk}(\omega)^* D^{(J)}_{MK}(\alpha, \beta, 0)^*\, |v\rangle, \tag{23}$$

where we suppress J and M in the short-hand notation on the left-hand side, since these quantum numbers are constant throughout the calculations. For the ν_3 mode the size of the basis is three times larger than for the other two vibrations because of the presence of the functions $|v\rangle = |\nu_3, m_l\rangle$ with $m_l = -1$, 0 and 1.

We have also computed line widths 2Γ directly by the golden rule formula, eqn. (22) in ref. 25,

$$\Gamma^{GR}_{\nu_3, w, K} = \pi \sum_{v, j, k} |\langle \Phi_{\nu_3, w, K}|\, W_{\nu_3, v}\, |\, \Phi_{v, j, k, K}(E)\rangle|^2. \tag{24}$$

The quasi-bound state $|\Phi_{\nu_3, w, K}\rangle$ is the specific Van der Waals state w of the ν_3 state that is excited by the photon. This state is here calculated as a bound eigenstate of the Hamiltonian in eqn. (21) with the monomer kinetic energy operator of eqn. (22). The function $|\Phi_{v, j, k, K}(E)\rangle$ is a scattering state of energy E, the energy of the $|\Phi_{\nu_3, w, K}\rangle$ state, that asymptotically correlates with the channel $|v, j, k, K\rangle$. The quantum number v indicates the ground and ν_1 states. The scattering states are obtained by coupled channel calculations with photodissociation boundary conditions in the ground and ν_1 state potentials. The operator $W_{\nu_3, v}$ coupling the scattering states v and the ν_3 states is that part of the intermolecular potential that is linear in $q_{3\alpha}$ for $v = 0$ and bilinear in $q_{3\alpha} q_1$ for $v = \nu_1$, *cf.* eqn. (8) to (12).

In eqn. (8) to (19) for the coupling terms in the potential we used the three Cartesian components of the normal coordinate $\boldsymbol{q}_3$. In the channel basis of eqn. (23) we introduced a spherical basis $|\nu_3, m_l\rangle$ for the ν_3 mode, which is more convenient for use with the operator $2\boldsymbol{l}^{vib}\cdot\boldsymbol{j}^{BF} = 2l_z^{vib} j_z^{BF} + l_+^{vib} j_+^{BF} + l_-^{vib} j_-^{BF}$ in eqn. (22). This spherical basis corresponds to the coordinates

$$(q_{3,1}, q_{3,0}, q_{3,-1}) = (q_{3x}, q_{3y}, q_{3z}) \begin{pmatrix} -1/\sqrt{2} & 0 & 1/\sqrt{2} \\ -\mathrm{i}/\sqrt{2} & 0 & -\mathrm{i}/\sqrt{2} \\ 0 & 1 & 0 \end{pmatrix}. \tag{25}$$

From the chain rule we find for the derivatives

$$\left(\frac{\partial}{\partial q_{3,1}}, \frac{\partial}{\partial q_{3,0}}, \frac{\partial}{\partial q_{3,-1}}\right) = \left(\frac{\partial}{\partial q_{3x}}, \frac{\partial}{\partial q_{3y}}, \frac{\partial}{\partial q_{3z}}\right) \begin{pmatrix} -1/\sqrt{2} & 0 & 1/\sqrt{2} \\ +\mathrm{i}/\sqrt{2} & 0 & +\mathrm{i}/\sqrt{2} \\ 0 & 1 & 0 \end{pmatrix}. \tag{26}$$

It is easily verified [*cf.* eqn. (12)] that

$$\sum_m \left(\frac{\partial A}{\partial q_{3m}}\right)_0 q_{3m} = \sum_\alpha \left(\frac{\partial A}{\partial q_{3\alpha}}\right)_0 q_{3\alpha}, \tag{27}$$

where the spherical components of $\boldsymbol{q}_3$ are indicated by m and the Cartesian by α. Equivalent relations exist between $(\partial^2 A/\partial q_{3\alpha}\partial q_1)_0$ and $(\partial^2 A/\partial q_{3m}\partial q_1)_0$. The terms in q_{3m} appearing in the potential couple the ground vibrational state with the ν_3 excited state. Similarly, the terms in q_1 couple the ground state with the ν_1 vibrational states, while the excited ν_1 and ν_3 states are mixed by the bilinear terms in $q_{3m}q_1$.

With regard to the dipole moment surface appearing in the cross section we point out that all intermolecular effects are neglected, so that the surface factorizes into a vibrational part and a part depending on the intermolecular coordinates:

$$\mu^{\mathrm{SF}}_{m''} = \sum_{m,\,m'} \mu_m(\boldsymbol{q}_3) D^{(1)}_{m'm}(\omega)^* D^{(1)}_{m''m'}(\alpha,\,\beta,\,0)^*. \tag{28}$$

The vibrational part $\mu_m(\boldsymbol{q}_3)$ appears in a matrix element coupling the $v = 0$ state with the ν_3 state. We simply take the intramolecular $v = 0 \rightarrow \nu_3$ transition moment of CH_4 as the unit of dipole moment, as was done earlier.[11] This is possible because we are only interested in relative line strengths. The vibrational part of the dipole is obviously of F_2 symmetry, otherwise the transition moment would be zero. The total dipole surface is of A_2 symmetry under $\mathrm{PI}(T_\mathrm{d})$ because it is invariant under permutations of identical nuclei and changes sign under space inversion E^*. Since F_1 is the only irrep giving A_2 when multiplied with F_2, the intermolecular part must be of F_1 symmetry. For the states of the dimer we have a similar symmetry rule. Since the ground vibrational state, as well as the ν_1 state, are of A_1 symmetry, the corresponding symmetry of the total dimer state is simply the symmetry Γ^{vdw} of its intermolecular part. However, for the ν_3 state we must consider the reduction $F_2 \otimes \Gamma^{\mathrm{vdw}}$ to find the symmetry of the total state. For example, for $\Gamma^{\mathrm{vdw}} = F_2$ we obtain $F_2 \otimes F_2 = A_1 \oplus E \oplus F_1 \oplus F_2$.

In the scattering calculations we compute matrix elements of the intermolecular potential between the channel functions of eqn. (23). The angular dependence of the potential is given in eqn. (8) to (10) by the expansion of both the linear and the exponential parameters in terms of tetrahedral harmonics $T^{(l)}_\gamma(\Theta, \Phi)$, which are linear combinations of spherical harmonics $Y^l_m(\Theta, \Phi)$. Matrix elements of spherical harmonics are easily computed by application of the Wigner–Eckart theorem, but not if they appear in the exponent. To tackle this problem we expanded the total intermolecular potential, including its exponential parts, in spherical harmonics $Y^\lambda_\mu(\Theta, \Phi)$. Obviously $\lambda_{\mathbf{max}} = 12$ is larger than $l_{\mathbf{max}} = 7$. We must then compute the following angular matrix elements:

$$\langle j',\, k',\, K \,|\, Y^\lambda_\mu \,|\, j,\, k,\, K\rangle, \tag{29}$$

which are proportional to products of two three-j symbols. The dependence of the intermolecular potential on the symmetrized C–H stretch coordinates $\boldsymbol{q}_3$ and q_1 is described by the Taylor expansion in eqn. (12). The matrix elements in these coordinates are simply

$$\begin{aligned} \langle \nu_3,\, m_l \,|\, q_{3m} \,|\, v = 0\rangle &= \delta_{m_l,\,m} h^{(\nu_3)}_{1,0} \\ \langle \nu_1 \,|\, q_1 \,|\, v = 0\rangle &= h^{(\nu_1)}_{1,0} \\ \langle \nu_3,\, m_l \,|\, q_{3m} q_1 \,|\, \nu_1\rangle &= \delta_{m_l,\,m} h^{(\nu_3)}_{1,0} h^{(\nu_1)}_{1,0} \end{aligned} \tag{30}$$

The matrix elements $h^{(v)}_{1,0}$ appearing here are the usual harmonic oscillator expressions.[30]

To end this section we mention some computational details. The maximum value of j in the angular channel basis was 9 in most cases. A substantially larger value of $j_{\mathbf{max}}$ was taken in the calculations referring to the direct dissociation of the ν_3 excited levels to ground state CH_4 and Ar, because of the large energy gap of 3019.5 cm^{-1} involved in this process which leaves ground state rotational channels open up to $j = 23$ inclusive. We then used $j_{\mathbf{max}} = 26$ for ground state CH_4. Bound states were calculated with the same Morse oscillator radial basis ($0 \leqslant n \leqslant 10$) and the same parameters as in ref. 11, with a 20-point Gauss–Laguerre quadrature for the radial integrals. Note that the energies of the present (quasi-)bound levels differ slightly from those in

ref. 11, because the fit of the SAPT potential surface described in Section 2 is more accurate than the fit of ref. 11. Dissociating states were propagated with the De Vogelaere algorithm[31,32] from $R = 4.5$ to 30 a_0 with step size 0.008 a_0. The bound wavefunctions involved in the photodissociation and the coupling terms in the potential were first computed with intervals varying from 0.05 a_0 for $4.5 \leqslant R/a_0 \leqslant 10$, to 0.5 a_0 for $R \leqslant 15$ a_0, to 1.0 a_0 for larger R, and then interpolated during the propagation. Resonances in the photodissociation cross sections were traced by performing coupled channel calculations for a range of energies with steps of 0.01 cm^{-1} and then characterized by zooming in on them, to a degree that depends on the width of the resonance.

4 Results

Before presenting the calculated results, let us briefly summarize the experimental findings. The high-resolution infrared spectrum of CH_4–Ar in the region of the ν_3 mode, measured by Miller and first presented at the 1994 Faraday Discussion on Van der Waals molecules,[9] is shown in Fig. 3. In ref. 11 it was found by means of an *ab initio* calculation of this spectrum that the seven bands (I to VII) in the experimental spectrum correspond to the transitions illustrated in Fig. 4. In Table 1 of ref. 12 it is shown that the widths of the lines in the different bands vary over an order of magnitude, despite the fact that the energies ($\approx$3020 cm^{-1}) of the transitions that correspond to these bands only vary over about 40 cm^{-1}.

From golden rule calculations for direct dissociation of the ν_3 excited complex into ground state CH_4 and Ar we found line widths $2\Gamma^{GR}$ that range from about 10^{-7} to 10^{-9} cm^{-1}, much smaller than the observed values. Hence, we must conclude that, because of the large energy gap involved in this process, the ground state channel effectively does not contribute to the ν_3 vibrational predissociation of the CH_4–Ar complex. We therefore omitted this channel altogether, and considered only decay into the channel in which the CH_4 fragment remains excited in the ν_1 mode. The second order terms in the potential that couple the ν_3 and ν_1 excited states are smaller by an order of magnitude than the direct (first order) coupling of ν_3 with the ground state, *cf.* Fig. 2 with Fig. 1, but the small kinetic energy release makes the ν_1 channel very effective in vibrational predissociation. This is clearly demonstrated by the results in Table 1, which contains the widths of the resonances in the photodissociation cross section corresponding to excitation of different ν_3 levels. These resonances, some of which are shown in Fig. 5, were found in calculations of the

Table 1 Transitions, see Fig. 4, corresponding to lines in the lowest three bands in the spectrum of Fig. 3. Energies of the ground state and ν_3 excited levels (in cm^{-1}) are relative to Ar and CH_4, ground state or ν_3 excited. In parentheses with the excited level is the symmetry of the Van der Waals state. The line widths 2Γ are obtained from fits of $\sigma_{f\leftarrow i}(E)$ to a Lorentzian line shape function. The two values in parentheses result from calculations in which the intermolecular potential, including the coupling terms, is scaled by a factor of 0.95 and 1.05, respectively. The latter value is missing from the first row because the scaling by 1.05 closes the corresponding channel for dissociation

Band	Ground state level	ν_3 excited level	Transition freq./cm^{-1}	reson. width, 2Γ/cm^{-1}	exper. line width/cm^{-1}
	$J, K = 1, 0 \rightarrow 0, 0$				
Ia	F_1	$F_2(A_1)$	3010.17	0.004	0.04?
	−82.99	−92.31		(0.006, —)	
II	F_1	$F_2(F_2)$	3019.61	0.004	0.001 to 0.006
	−82.99	−82.88		(0.011, 0.006)	
IIIa	A_2	$A_1(F_2)$	3027.36	0.014	>0.01
	−92.10	−84.23		(0.080, 0.004)	
	$J, K = 0, 0 \rightarrow 1, 1$				
II	F_2	$F_1(F_2)$	3019.72	0.0005	0.001 to 0.006
	−83.18	−82.95			
II	F_2	$F_1(F_2)$	3020.77	0.003	0.001 to 0.006
	−83.18	−81.89			

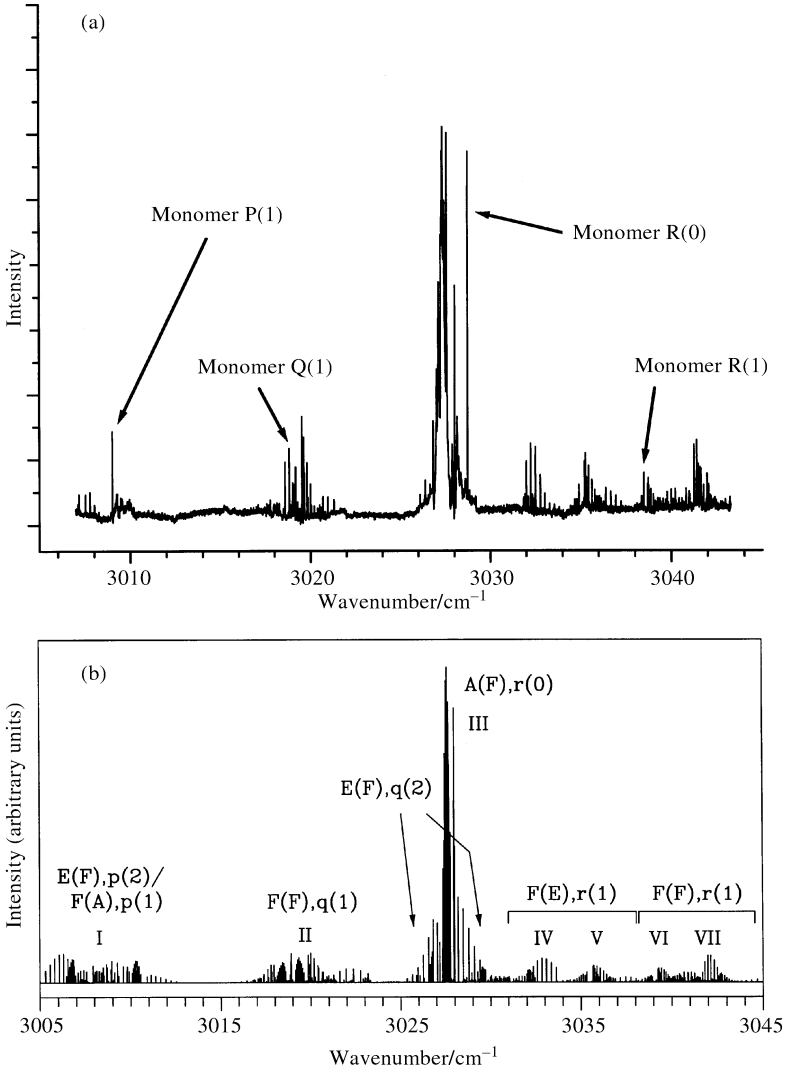

Fig. 3 (a) Broad scan of experimental infrared spectrum of CH_4–Ar. (b) *Ab initio* calculated spectrum at $T = 1$ K from ref. 11. The symmetry species is indicated; initial and final states are of the same symmetry. Between parentheses is the symmetry of the Van der Waals component of the final state. The symbols p(*j*), q(*j*) and r(*j*) refer to transitions from an initial state of certain *j*, the angular momentum of the methane monomer. The labeling I to VII of the bands corresponds to the transitions indicated in Fig. 4.

cross sections for the excitation of different ν_3 levels from various ground state Van der Waals levels, followed by decay into the rotational levels of ν_1 excited CH_4 fragments that are energetically accessible. Since these line widths range from about 0.001 to more than 0.01 cm^{-1}, in good agreement with the observed values, we conclude that the fragmentation into Ar and ν_1 excited CH_4 is indeed the dominant dissociation channel.

Other possible channels involving intermediate states with CH_4 excited into the lower lying ν_2 and ν_4 bending modes, overtones, or combinations, were not explicitly considered in this work. Due to the relatively large energy releases and the even more indirect couplings required for dissociation through 'doorways' involving these modes, we believe that they are much less effective than the ν_1 mode. An experimental result that supports this conclusion is that the lines in the ν_4 excitation spectrum of the CH_4–Ar complex[33] do not show any life time broadening. The ν_4

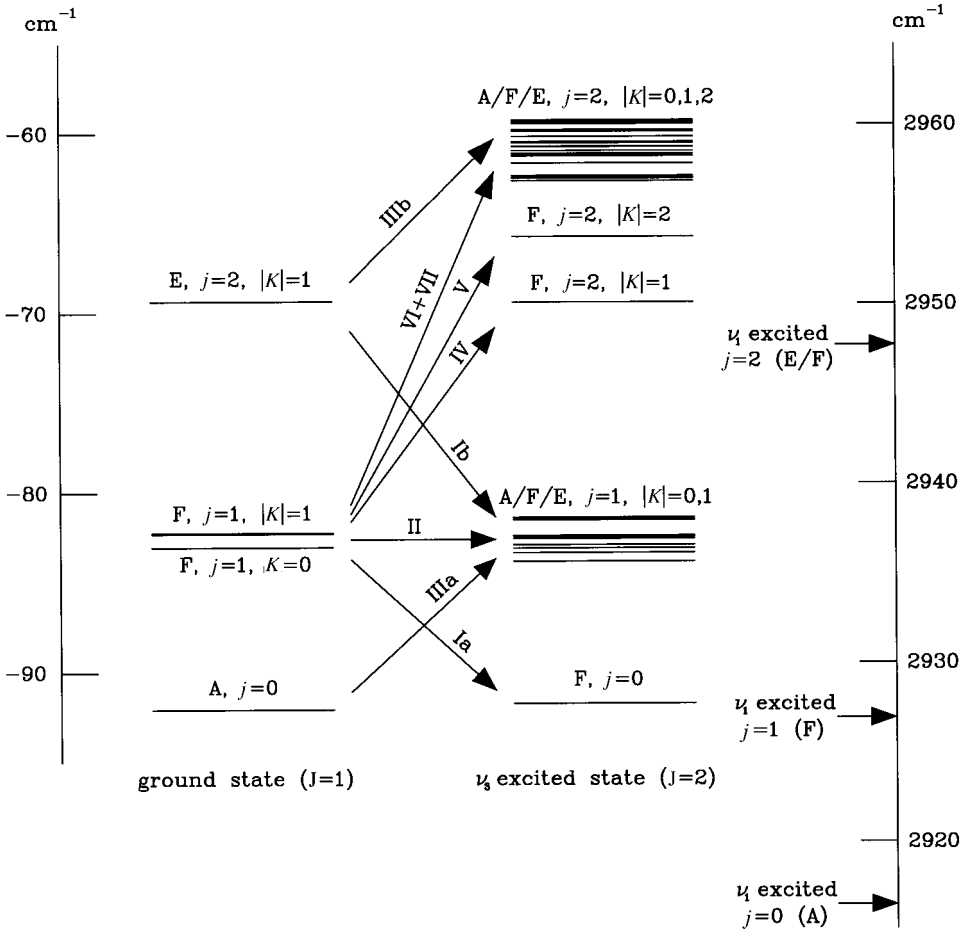

Fig. 4 Transitions between ground and excited state levels of CH_4–Ar, leading to the bands I to VII shown in Fig. 3. For clarity we depicted only the ground state levels with $J = 1$ and the excited state levels with $J = 2$. On the scale of the excited state energies we marked the thresholds for photodissociation of the A, F and E species into argon and ν_1 excited methane.

vibration at 1310.76 cm^{-1} is the lowest frequency mode of CH_4 and there are no levels available that would allow the complex to dissociate with such a small kinetic energy release as the ν_1 'doorway' does for the ν_3 excitations.

Our calculations of the photodissociation cross section $\sigma_{f\leftarrow i}(E)$ are presently limited to the ν_3 excited levels below 2940 cm^{-1} relative to Ar and ground state CH_4, *i.e.*, to the bands I, II and IIIa below 3030 cm^{-1} in the spectrum of Fig. 3. Interesting resonances occur already in this region, in particular those illustrated in Fig. 5, which we will now discuss in more detail. The energy dependence of all of the resonant cross sections could be precisely fit by a Lorentzian line shape function, which allowed us to extract accurate line widths (excited state life times). All of the excited levels in the resonant transitions shown in Fig. 5 originate from a specific Van der Waals level of the complex with F_2 symmetry for $J = 0$ (F_1 for $K = 0$ and odd J, and both F_1 and F_2 for $|K| > 0$). In combination with the threefold degenerate ν_3 mode of F_2 symmetry this Van der Waals level gives rise to four levels: one of A_1, one of F_1, one of F_2, and one of E symmetry (for $J = 0$). The splitting between these levels is caused by the intermolecular potential and by the first-order Coriolis coupling between the vibrational angular momentum l of the ν_3 mode and the hindered rotation j of the CH_4 monomer in the complex, see eqn. (22). The typical splitting pattern of these levels, indicated by the dashed bars in Fig. 5, was already observed and explained in

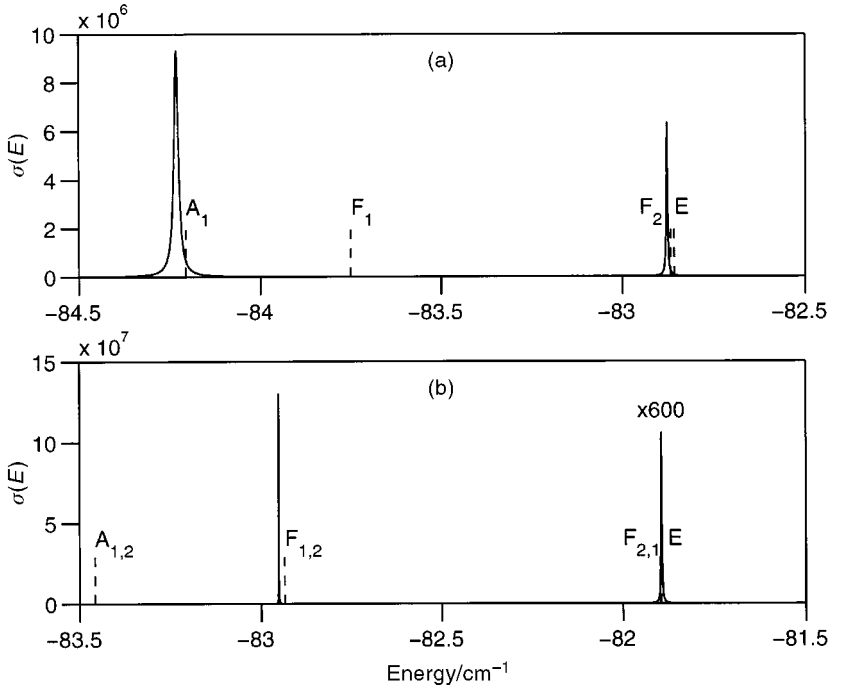

Fig. 5 Resonances in the cross sections (in atomic units) for excitation to different quasi-bound levels in the ν_3 excited state of CH_4–Ar. The dashed bars indicate the corresponding quasi-bound levels calculated by omission of the open ν_1 channels. (a) $J,K = 1,0 \rightarrow 0,0$ transitions to quasi-bound levels of A_1 and F_2 symmetry. (b) $J,K = 0,0 \rightarrow 1,1$ transitions to quasi-bound levels of F_1 and F_2 symmetry.

ref. 11. It is based on the fact that for the A and F species the internal rotation is only slightly hindered so that j is still a nearly good quantum number. The F_2 Van der Waals level relevant here belongs to $j \approx 1$ and, in combination with $l = 1$, this gives rise to the approximate quantum number r belonging to the angular momentum operator $\boldsymbol{r} = \boldsymbol{j}^{BF} - \boldsymbol{l}^{vib}$. The A_1 level corresponds to $r \approx 0$, the F_1 level to $r \approx 1$ and the F_2 and E levels to $r \approx 2$. The $r = 1$–0 splitting is $2\zeta_3 B_3 \approx 0.5\ cm^{-1}$ and the $r = 2$–1 splitting is $4\zeta_3 B_3 \approx 1.0\ cm^{-1}$. This splitting pattern was clearly recognized in the quasi-bound levels computed in ref. 11, where it was further observed that the splitting between the F_2 and E levels caused by the anisotropy of the intermolecular potential is much smaller.

The same splitting pattern can be recognized for the resonances displayed in Fig. 5, but not all symmetry components appear. As mentioned above, we considered the ν_3 excited levels below $2940\ cm^{-1}$. Only ν_1 excited channels with $j = 0$ and $j = 1$ are open at this energy, *cf.* Fig. 4; they correspond to symmetries A_1 and F_2, respectively (for $J = 0$). Hence, for $J = K = 0$ the ν_3 excited levels of F_1 and E symmetry cannot couple to the ν_1 continuum and do not yield resonances in our calculations. Further restrictions are due to the selection rules: $A_1 \leftrightarrow A_2$, $F_1 \leftrightarrow F_2$, $E \leftrightarrow E$, dictated by the A_2 symmetry of the transition dipole operator, and the symmetry of the ground state levels from which the transitions originate. The two resonances in the $J, K = 1, 0 \rightarrow 0, 0$ transitions in Fig. 5(a) correspond to the quasi-bound levels of A_1 and F_2 symmetry, separated by about $1.5\ cm^{-1}$. The A_1 resonance is accessed from a $J = 1$ ground level of A_2 symmetry, while the F_2 resonance is excited from a $J = 1$ ground state level of F_1 symmetry. The first transition corresponds to a line in band IIIa of the spectrum, the second to a line in band II. In the J, $K = 0, 0 \rightarrow 1, 1$ transitions in Fig. 5(b) one observes also the $(J = 0)$ resonance of F_1 symmetry, which is excited together with the F_2 resonance. The two peaks are indeed separated by about $1.0\ cm^{-1}$. For $|K| = 1$ both these resonances have obtained F_1 and F_2 components; the F_1 components are those that are actually excited from a ground state $(J = K = 0)$ level of F_2 symmetry.

Both transitions correspond to lines in band II of the spectrum. The A_1 resonance is absent from the calculated spectrum in Fig. 5(b) because there are no continuum states of A symmetry in the ν_1 excited channel that can couple with the ν_3 level of A_1 symmetry to broaden this level into a resonance. The ν_1 channel of A_1 symmetry with $j = 0$ that was open for $K = 0$ does not occur for $K = 1$ because of the condition $j \geqslant |K|$.

The variation in their widths, see Table 1, is what makes these resonances so interesting. The lines in band IIIa of the experimental spectrum are very broad (>0.01 cm^{-1}), so that the individual lines overlap and can no longer be identified. The lines in band II are much narrower. A more detailed analysis[34] of the various lines in this band revealed that their widths vary between 0.001 and 0.006 cm^{-1}. This substantial difference in line width is remarkable since the ν_3 levels excited in bands II and IIIa correspond to the same ($j \approx 1$) Van der Waals level of F symmetry, *cf.* Fig. 4. The resonances in our calculated photodissociation cross sections nicely reflect the measured variations: the band IIIa transition to a resonance of A symmetry is indeed broader than 0.01 cm^{-1}, while the transitions to resonances of F symmetry (band II) have widths between 0.0005 and 0.004 cm^{-1}.

From the results in Table 1 it seems that the widths of the lines in band I agree less well with experiment, but it should be noted that this band consists of two subbands, one with very narrow lines and one with broad lines, and that the measured lines in this band could not be individually assigned yet.

An interesting observation is that the resonance widths are extremely sensitive to the potential surface. This was investigated by a global scaling of the potential by factors of 0.95 and 1.05 which gave markedly different resonance widths, see Table 1. Not shown in the table is that, of course, the positions of the resonances shift as well. One of the origins of the width changes is the change in the coupling matrix elements between the ν_3 channels and the open ν_1 channels that is a consequence of scaling the potential, but we found an even more important reason for the sensitivity of the resonance widths. The small kinetic energy release associated with dissociation into the ν_1 channel implies that the quasi-bound ν_3 levels couple with the low lying part of the ν_1 continuum, up to about 60 cm^{-1}. Upon investigation of this continuum we found that for such low energies there is a marked resonance structure, probably due to rotational predissociation. The amount of broadening of a quasi-bound ν_3 level depends strongly on how close it is to such resonances in the ν_1 continuum. The same effect was found[35] in the vibrational predissociation of the triatomic Ne–Br_2 Van der Waals complex, when the $\Delta v = -1$ channel was open with little available energy. We confirmed this conclusion by scaling the potential of the ν_3 state only, while leaving the potential of the ν_1 state and the coupling terms unaffected.

Also the result that the resonance widths of ν_3 states of different A, F and E symmetry are so different is related to the fact that the resonance structure in the ν_1 continuum depends strongly on the symmetry. The ν_1 channels of different symmetries open up at different thresholds; we saw this already for the $j = 0$ and $j = 1$ channels which correspond to symmetries A_1 and F_2, respectively (for $J = 0$). A further investigation into the relation between the resonances in the ν_1 continuum and the widths of the ν_3 excited levels is in progress. Also the extension of our calculations to higher ν_3 levels (bands IV to VII in the spectrum) will be performed shortly. This extension will also involve the levels of E symmetry; we expect that it will provide further interesting material.

Our photodissociation calculations also provide the distribution of the ν_1 excited CH_4 fragment over rotational states. For the lower ν_3 excited levels that we calculated up to now this distribution is very simple. The only ν_1 channels open are $j = 0$ and $j = 1$. Excitation to a $K = 0$ level of A_1 or A_2 symmetry, for even and odd J, respectively, yields the pure $j = 0$ product. Excitation to a level of F_2 or F_1 symmetry, for even and odd J, yields pure $j = 1$. For $|K| = 1$ the ν_1 channel with $j = 0$ is absent and the $j = 1$ channel has both F_2 and F_1 components. For $|K| > 1$ no dissociation occurs upon excitation of these lower ν_3 excited levels. The inclusion of Coriolis coupling which mixes the states with different K will make these rules somewhat less strict.

5 Conclusion

This paper describes a calculation, completely *ab initio*, of the energy dependent cross section for vibrational predissociation of CH_4–Ar through excitation of the ν_3 asymmetric stretch mode of CH_4. It is based on an intermolecular potential surface that depends explicitly on the ν_3 and ν_1

normal coordinates of the CH_4 monomer, obtained from electronic structure calculations by SAPT. Particular attention is given to the widths of the resonances in this cross section which correspond to various quasi-bound Van der Waals levels excited in combination with the ν_3 mode. It is found that dissociation into CH_4 fragments excited in the ν_1 symmetric stretch mode strongly dominates over direct dissociation into ground state CH_4, and is responsible for the strong line broadening observed experimentally. The efficiency of this $V \rightarrow V'$ process is caused by a very low kinetic energy release. Good agreement with the measured high-resolution spectrum is obtained, both for the magnitude of the line widths and for their variation over different quasi-bound levels.

Furthermore, it is found that the widths of the resonances in the photodissociation cross section depend extremely sensitively on the potential surface. This strong dependence is related to the occurrence of rotational predissociation resonances in the low-lying continuum of the ν_1 state in the same energy range as the quasi-bound ν_3 levels. Also the large differences in the resonance widths for ν_3 levels of A, F and E symmetry are related to the opening up of ν_1 dissociation channels of different symmetry and the resonance structure in the lower range of the ν_1 continuum.

Acknowledgement

We thank Professor Roger Miller for stimulating discussions. We acknowledge travel support through the Van Gogh program of the Netherlands Organization for Scientific Research (NWO) and the French Ministry of Foreign Affairs (Action Intégrée Van Gogh 98023).

References

1 J. M. Hutson, D. C. Clary and J. A. Beswick, *J. Chem. Phys.*, 1984, **81**, 4474.
2 A. Rohrbacher, J. Williams and K. C. Janda, *Phys. Chem. Chem. Phys.*, 1999, **1**, 5263.
3 A. Rohrbacher, N. Halberstadt and K. C. Janda, *Annu. Rev. Phys. Chem.*, 2000, **51**, 405.
4 C. Bissonnette and D. C. Clary, *J. Chem. Phys.*, 1992, **97**, 8111.
5 D. J. Nesbitt and R. Lascola, *J. Chem. Phys.*, 1992, **97**, 8096.
6 R. Lascola and D. J. Nesbitt, *J. Chem. Phys.*, 1991, **95**, 7917.
7 R. Moszynski, P. E. S. Wormer and A. van der Avoird, in *Computational Molecular Spectroscopy*, ed. P. R. Bunker and P. Jensen, Wiley, New York, 2000, p. 69.
8 A. R. W. McKellar, *Faraday Discuss.*, 1994, **97**, 69.
9 R. E. Miller, *Faraday Discuss.*, 1994, **97**, 177.
10 D. J. Nesbitt, *Faraday Discuss.*, 1994, **97**, 175.
11 T. G. A. Heijmen, P. E. S. Wormer, A. van der Avoird, R. E. Miller and R. Moszynski, *J. Chem. Phys.*, 1999, **110**, 5639.
12 R. E. Miller, T. G. A. Heijmen, P. E. S. Wormer, A. van der Avoird and R. Moszynski, *J. Chem. Phys.*, 1999, **110**, 5651.
13 T. G. A. Heijmen, T. Korona, R. Moszynski, P. E. S. Wormer and A. van der Avoird, *J. Chem. Phys.*, 1997, **107**, 902.
14 T. G. A. Heijmen, R. Moszynski, P. E. S. Wormer, A. van der Avoird, U. Buck, C. Steinbach and J. M. Hutson, *J. Chem. Phys.*, 1998, **108**, 4849.
15 S. Green, *Chem. Phys.*, 1979, **40**, 1.
16 T. A. Brunner and D. E. Pritchard, *Adv. Chem. Phys.*, 1982, **50**, 589.
17 J. T. Hougen, in *International Review of Science*, ed. D. A. Ramsay, Butterworth, London, 1976, vol. 3, p. 75.
18 E. B. Wilson, J. C. Decius and P. C. Cross, *Molecular Vibrations*, McGraw-Hill, New York, 1955.
19 D. Papoušek and M. R. Aliev, *Molecular Vibrational–Rotational Spectra*, Elsevier, Amsterdam, 1982.
20 L. C. Biedenharn and J. D. Louck, *Angular Momentum in Quantum Physics*, Addison-Wesley, Reading, 1981.
21 Tang Au-Chin, *Theoretical Method of the Ligand Field Theory*, Science Press, Beijing, 1979.
22 P. E. S. Wormer and H. Hettema, *J. Chem. Phys.*, 1992, **97**, 5592.
23 K. T. Tang and J. P. Toennies, *J. Chem. Phys.*, 1984, **80**, 3726.
24 C. G. Gray and A. G. Robiette, *Mol. Phys.*, 1979, **37**, 1901.
25 O. Roncero, J. A. Beswick, N. Halberstadt, P. Villarreal and G. Delgado-Barrio, *J. Chem. Phys.*, 1990, **92**, 3348.
26 E. Venuti, L. Halonen and R. G. Della Valle, *J. Chem. Phys.*, 1999, **110**, 7339.
27 G. Tarrago, M. Dang-Nhu, G. Poussigue, G. Guelachvili and C. Amiot, *J. Mol. Spectrosc.*, 1975, **57**, 246.
28 J. E. Lolck and A. G. Robiette, *Chem. Phys. Lett.*, 1979, **64**, 195.

29 *Handbook of Chemistry and Physics*, ed. R. C. Weast and M. J. Asth, CRC Press, Boca Raton, FL, 1981.
30 A. Messiah, *Quantum Mechanics*, North Holland, Amsterdam, 1969, vol. 2.
31 W. Lester, *J. Comput. Phys.*, 1968, **3**, 322.
32 W. Lester, *Methods Comput. Phys.*, 1971, **10**, 211.
33 I. Pak, D. A. Roth, M. Hepp, G. Winnewisser, D. Scouteris, B. J. Howard and K. M. T. Yamada, *Z. Naturforsch. A*, 1998, **53**, 725.
34 R. E. Miller, personal communication, 2000.
35 T. A. Stephenson and N. Halberstadt, *J. Chem. Phys.*, 2000, **112**, 2265.